Electrokinetic flow in a free surface-guided microchannel

Jacky S. H. Lee, Irena Barbulovic-Nad, Zhemin Wu, Xiangchun Xuan, and Dongqing Li[a)]
Department of Mechanical and Industrial Engineering, University of Toronto, 5 King's College Road, Toronto, Ontario M5S 3G8, Canada

(Received 13 September 2005; accepted 26 January 2006; published online 7 March 2006)

The purpose of this study is to investigate electro-osmotic flow in a free surface-guided microchannel. Although multiphase microfluidics has attracted interests over the past few years, electro-osmotic flow involving free surfaces has yet to be studied in great detail. Several proposed theoretical models describing this type of electro-osmotic flow need to be verified by experiments. In this work, a surface-guided microchannel was fabricated using an innovative fabrication process. Because the liquid stream was confined by surface properties, solid sidewalls did not exist in this microchannel. Instead, the sidewalls were water-air or water-oil interfaces. Using this microchannel, two systems were investigated: water-air system and water-oil system. The experimental results were compared against three proposed models in order to gain more understandings on this type of electro-osmotic flow. Experimental results show that the liquid velocity near the liquid-fluid interface resembles a pluglike profile for both water-air and water-oil systems. Computer simulation results show that with the consideration of the electrical double layer and the surface charges, the electric forces inside the electrical double layer are counteracted by the surface forces at the liquid-fluid interface, also resulting in a pluglike velocity profile in the microchannel. Therefore, the model that considers both the electrical double layer and the surface charges at the liquid-fluid interface best describe the physical phenomenon observed in experiments. © *2006 American Institute of Physics*. [DOI: 10.1063/1.2177428]

I. INTRODUCTION

Electro-osmotic flow is one of the most common means of liquid transport in microfluidic devices. Over the past decades, researchers have focused on the fundamentals and applications of electroosmotic flow in microchannels.[1–7] Electro-osmotic flow is known for its pluglike velocity profile, which is advantageous to sample transport processes such as capillary electrophoresis.[8,9] Electro-osmotic flow can be easily controlled by applied electric fields, allowing for precise liquid manipulation in a complex microchannel network. Examples include liquid dispensing[10] in a cross-shape microchannel.

Most studies on electro-osmotic flow were focused on glass or polymer microchannels. These typical microchannels might have varying cross-sectional shapes, but the liquid inside these microchannels all completely enclosed by solid surfaces. The origin of electro-osmotic flow in such microchannels can be well explained by the widely accepted Gouy-Chapman-Stern model, which describes the formation of an electrical double layer (EDL) in the proximity of a liquid-solid interface.

The recent advancement in microfluidics has led to investigations on two-phase systems at microscale. Most of these systems involved oil droplet transport in microchannels.[11–13] Recently, investigations on using a two-phase system to indirectly pump nonpolar liquid electrokinetically were conducted.[14–16] Overall, the fundamental understandings of electrokinetic flow involving two fluid phases in microchannels are currently insufficient. There have been very little discussions on the physics of electrokinetic flow near an interface of two immiscible fluids (i.e., water-air or water-oil system). Brask *et al.*[14] and Gao *et al.*[16] have theoretically investigated on a two-phase electro-osmotic flow; however, both authors conducted their theoretical studies using different assumptions at the liquid-fluid interface without any supporting evidence and justification. Therefore, fundamental research, such as the determination of the proper theoretical models and experimental demonstrations on electro-osmotic flow involving two immiscible fluids, is necessary.

This paper presents a fundamental investigation on electro-osmotic flow in free surface-guided microchannels. An innovative fabrication method was developed, in which both the inner surfaces of the top and the bottom glass plates could be patterned simultaneously. The straight microchannel used in the experiments was defined by the hydrophobic and hydrophilic patterns on both the top and the bottom glass surfaces using a self-assembled monolayer (SAM) called octadecyltrichlorosilane (OTS) where the patterns were created by selective deep-ultraviolet (deep-UV) exposure. The resulting liquid channel had two free surfaces as the sidewalls, and the liquid could be in contact with air or other immiscible liquids. Similar microchannels containing free surface sidewalls have been previously developed. Zhao *et al.*[17–19] created what is called a "surface-directed" liquid channel by using a photocleavable SAM formed on the channel's inner surfaces. Bouaidat *et al.*[20] created their surface-directed liq-

[a)]Author to whom correspondance should be addressed; present address: Department of Mechanical Engineering, Vanderbilt University, Nashville, TN 37235; electronic mail: dongqing.li@vanderbilt.edu

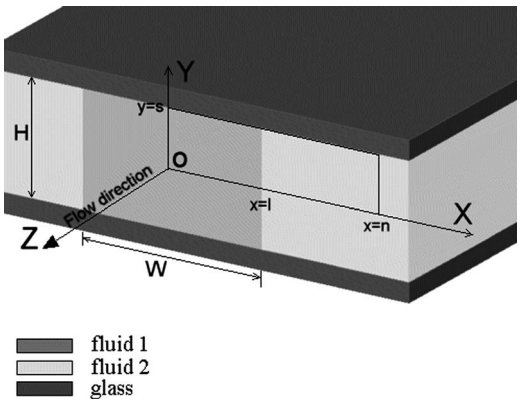

FIG. 1. The schematic of the coordinate system. Computational domain enclosed by the rectangular enclosure. $x=l$ denotes the location of the fluid interface. $x=n$ denotes fluid 2 outer boundary. $y=s$ is the location of the glass surface.

uid channel by only forming a hydrophilic/hydrophobic pattern on the bottom glass surface while the top glass surface was completely hydrophobic. Although the basic concept of channel fabrication used in our experiments is similar to that of Zhao *et al.*, the method proposed in this paper only involves OTS coatings and does not require the chemical procedures that are needed to create the photocleavable SAM. In our experiments, the liquid velocity was measured by the particle streak method. Experimental results were then compared with three proposed theoretical models in an attempt to explain the physical phenomena.

II. THEORY

The planar geometry investigated in this work is shown in Fig. 1. Two fluid phases are considered, and liquid flow $u(x,y)$ is in the positive z direction. The top and bottom surfaces are glass while the free surface sidewall is the interface between the two immiscible fluids. The width of fluid stream 1 is denoted by W and the height of the channel is denoted by H. To simplify the model, the interface between the two immiscible fluids is assumed to be flat. Additionally, we consider constant liquid properties such as density, viscosity, and electrical permittivity. Fluid flow is considered to be fully developed and in steady state. In this study, three different models were tested. All three models use the Poisson-Boltzmann distribution to describe the electrical double layer and the Stokes equation to describe the fluid flow. The only difference between the three models is the treatment of the liquid-fluid interface boundary conditions. The first model (μ model), proposed by Brask *et al.*,[14] considers purely the viscous forces between two immiscible fluids and does not consider any electrical double layer effect at the liquid-fluid interface. In their treatment of boundary conditions, there is no zeta potential assigned to the liquid-fluid interface; however, the continuity of shear stress applies in the flow calculation. The second model (EDL model), proposed by Gao *et al.*,[16] includes the consideration of electrical double layer at the liquid-fluid interface. In this model, a zeta potential is assigned to the liquid-fluid interface and the Poisson-Boltzmann equation is solved for the EDL field. For the fluid flow, the continuity of shear stress is applied at the liquid-fluid interface, similar to the model of Brask *et al.* The third model (EDL+SC model), based on a modification of the model of Gao *et al.*, includes the consideration of both the electrical double layer and the surface charges at the liquid-fluid interface. The electric charges at this interface will experience electric forces under an applied electric field. Since the surface charges at this interface and the net charges in the electrical double layer are opposite in sign, the resulting liquid-fluid interface motion and the EDL motion are in the opposite direction. Thus, while the liquid inside the electrical double layer moves forward due to the electric forces, it is also being "pull back" or drag by the moving interface due to the counteracting forces from the surface charges. This model, which considers these two forces near the liquid-fluid interface, may predict a very different velocity profile compared to the two previous models. Mathematically, the EDL+SC model and the EDL model provide a different boundary condition on the EDL field. It is only very recently that the authors are aware of that Gao *et al.* (very recently published)[21] have also improved their model to consider the surface charges in their analysis of an electro-osmotic two-phase flow.

A. The electrical double layer (EDL)

Generally, all surfaces in contact with water or an aqueous solution carry electric charges. Due to these charges, an electrical double layer is formed near the surface.[22] The electrical double layer can be described by the well-known Poisson-Boltzmann equation

$$\bar{\nabla}^2\Psi = \kappa^2 a^2 \sinh \Psi, \tag{1}$$

where the dimensionless electrical potential and the Debye-Hückel parameter are defined as $\Psi = ze\psi/k_BT$ and $\kappa^2 = 2z^2e^2n_\infty/\varepsilon\varepsilon_0 k_BT$, respectively. The gradient operator is nondimensionalized as $\bar{\nabla} = a\nabla$, where a is the characteristic length denoted by $a = 2(W\times H)/(W+H)$ (i.e., the hydraulic diameter). The local net charged density ρ_e in the EDL for symmetric electrolyte is given by the Boltzmann distribution:

$$\rho_e = -2zen_\infty \sinh \Psi. \tag{2}$$

The parameters used in the above two equations include electrical potential ψ, the valence of ions z, elementary charge e, bulk ionic concentration n_∞, Boltzmann constant k_B, temperature T, absolute electrical permittivity ε_0, relative electrical permittivity ε, and characteristic length a. Generally, boundary conditions used in these models include $\Psi_{y=s} = ze\zeta_s/k_BT$ at the channel wall, $\Psi_{x=l} = ze\zeta_l/k_BT$ at the liquid-fluid interface, and $\vec{n}\cdot\bar{\nabla}\Psi = 0$ at the symmetrical boundaries ($x=0$, $y=0$), where $\vec{n}$ is the outward unit normal. There is one exception for the μ model, where $\Psi_{x=l}=0$ due to the assumption of a neutral interface. It should be noted that the EDL exists only in the side of the polar liquid.

B. Fluid flow

In general, the momentum equation that governs steady state, incompressible electro-osmotic flow is given by

$$\rho(\vec{u}\cdot\nabla)\vec{u} = -\nabla p + \mu\nabla^2\vec{u} + \rho_e\vec{E}, \tag{3}$$

where the fluid velocity $\vec{u}$ is dependent on the pressure p, density ρ, viscosity μ, local net charged density ρ_e, and the applied electric field $\vec{E}$. For the geometry shown in Fig. 1, by assuming pure electro-osmotic flow (no pressure gradient), the flow in fluid 1 can be described by the following expression:

$$\bar{\nabla}^2 U_1 + G\sinh\Psi = 0. \tag{4}$$

In fluid 2, the fluid flow is simply described by the Laplace equation without the consideration of the electrical body forces:

$$\bar{\nabla}^2 U_2 = 0. \tag{5}$$

In the above, parameters are defined as $U_{1,2}=u_{1,2}/u_{\mathrm{ref}}$ and $G=-2a^2zen_\infty E_z/\mu_1 u_{\mathrm{ref}}$, where E_z is the applied electric field strength in the z direction. The reference velocity u_{ref} is defined by the Helmholtz-Smoluchowski electro-osmotic velocity of $-\varepsilon\varepsilon_0\zeta_s E_z/\mu_1$.

The boundary conditions that are used for all three models include $U_{1,2}=0$ at the solid surface, $\vec{n}\cdot\bar{\nabla}U_{1,2}=0$ for the symmetrical boundaries, and $U_2=0$ at the fluid 2 outer boundary ($x=n$). The liquid-fluid interface boundary conditions must satisfy mass conservation and the continuity of shear stress. These conditions for the three models are summarized as follows:

(μ model): $U_1 = U_2$,

$$\vec{n}\cdot(\bar{\nabla}U_1 - \beta\bar{\nabla}U_2) = 0 \quad \text{recalled } \Psi_{x=l} = 0, \tag{6}$$

(EDL model): $U_1 = U_2$,

$$\vec{n}\cdot(\bar{\nabla}U_1 - \beta\bar{\nabla}U_2) = 0 \quad \text{recalled } \Psi_{x=l} = ze\zeta_l/k_BT, \tag{7}$$

(EDL + SC model): $U_1 = U_2$,

$$\vec{n}\cdot(\bar{\nabla}U_1 - \beta\bar{\nabla}U_2) = H \quad \text{recalled } \Psi_{x=l} = ze\zeta_l/k_BT, \tag{8}$$

where $\beta=\mu_2/\mu_1$, $H=a\sigma_s E_z/u_{\mathrm{ref}}\mu_1$, and the outward unit normal $\vec{n}$ is pointing from fluid 1 to fluid 2 at the interface. σ_s is the surface charged density at the interface and is expressed by $\sigma_s=\vec{n}\cdot(\varepsilon\varepsilon_0\nabla\psi|_{x=l})$ according to the theory of electrostatics. As described earlier, both the μ model and the EDL model use the continuity of shear stress as the boundary condition at the liquid-fluid interface. However, the EDL model assumes that there exists an EDL at the interface while the μ model does not. The extra term H in the EDL+SC model arises from the consideration of the surface charges at the liquid-fluid interface.

Numerical method

A high order finite difference scheme was used to solve the EDL and momentum equations. A nonuniform spaced grid was employed for more accurate solutions. A fine grid was used inside and near the EDL and liquid-fluid interface regions while the bulk flow region had a coarser grid. Different grid sizes have been tested to ensure that the grid independent solution was obtained. The total number of nodes used in the computation was 160 000. The set of discretized, partial differential equations was solved using a line-by-line iteration scheme combined with a tridiagonal matrix algorithm (TDMA) solver.

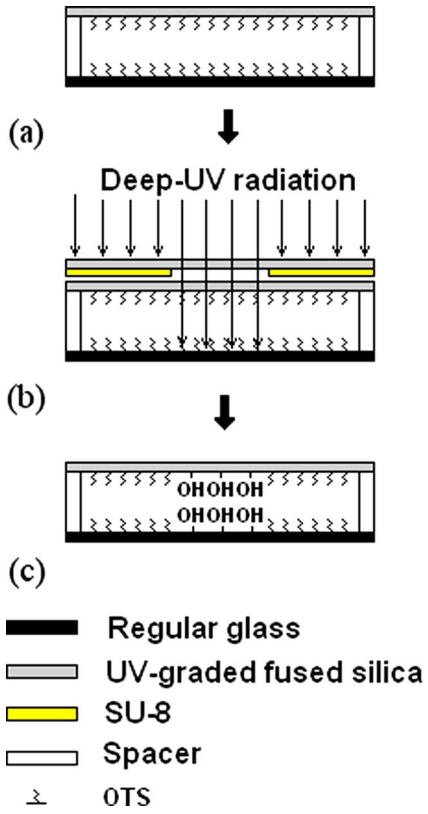

FIG. 2. (Color online) The fabrication process of the microchip. (a) Glass slides were treated with self-assembled monolayer OTS to become hydrophobic and were separated by spacers to form a microchip. (b) Deep-UV radiation penetrated the photomask into the microchip, where both the top and bottom inner surfaces were exposed to deep-UV radiation. OTS was removed in the regions exposed to deep UV. (c) After OTS was removed, the exposed regions became hydrophilic with hydroxyl surface group.

MICROCHANNEL FABRICATION

The microchannel used in the experiments was fabricated using an innovative process, in which a hydrophilic pattern was simultaneously created on both the top and the bottom OTS-coated glass surfaces of the microchannel via deep-UV/ozone exposure. OTS was chosen as the hydrophobic coating chemical due to the ease of coating steps as well as its excellent ability to be removed upon deep-UV exposure.[23,24] Two microscope slides of different glass materials were used in the fabrication. One is a regular 2×1 in.^{2} microscope glass slide, which could be purchased in most medical supply stores. The second type of slides requires deep-UV transmittance. The S1-UV fused silica graded 2×1 in.^{2} microscope slide (Esco Products Inc., Oak Ridge, NJ) was chosen because of its high UV transmittance down to deep UV. The fabrication steps are shown in Fig. 2 and are summarized as follows. Both the regular and UV-graded slides were coated with OTS to become hydrophobic. The glass microchip was formed by clamping the glasses

together with spacers in between. A photomask was placed on the top of the microchip with the UV-graded glass facing the photomask. This arrangement allowed the penetration of deep-UV radiation into the inner surfaces of the microchip. When selected regions on the inner surfaces were exposed to deep-UV radiation, the OTS on these regions was removed and hydrophilic properties were recovered. In this way, a hydrophilic surface-guided microchannel pattern was created on the top and the bottom inner surfaces simultaneously. A detailed fabrication steps are provided in subsequent sections.

Prior to chemical treatment, two 1/8 in. holes were drilled into the regular glass slide to be the reservoirs. Next, both the regular and UV-graded slides were cleaned and treated sequentially with 1*M* NaOH and 1*M* HCl solutions in ultrasonic bath for 20 and 10 min, respectively. After the treatment, the microscope slides were dried under compressed nitrogen gas. Once the slides were cleaned and hydrolyzed, they were submerged in a 1:200 v/v OTS:hexane solution for 5 min to form the OTS coating. Once the coating procedure was completed, the slides were washed and rinsed with acetone in ultrasonic bath for 2 min to remove any OTS residue left on the glass surfaces. At this moment, both slides were completely hydrophobic (contact angle larger than 100°). Upon the removal of the slides from the acetone solution, compressed nitrogen gas was used to immediately blow off any acetone on the surfaces, as the acetone was quickly evaporated. After the slides were coated with OTS solution, spacers were placed between the two glasses (Small Parts Inc., Miami Lakes, FL) and the glasses were clamped together using metal clips. Metal clips were used in the fabrication instead of adhesive because these slides could be cleaned and reused, reducing the costs of experiment. Attention must be paid to the creation of the photomask used in this experiment. Normally for photolithography in microfluidics, photomasks could be made by using laser printout on transparencies. However, in this fabrication method, this type of photomask could not be used because the transparencies absorb deep-UV radiation. Therefore, other types of photomask must be used. In this fabrication method, the photomask was created by spin coating a layer of SU-8 photoresist onto an UV-graded slide. Using common photolithography procedures,[25] a photoresist pattern was created on the UV-graded slide. This slide was used as the photomask because SU-8 could effectively block deep-UV radiation.[26] After placing the photomask on the top of the microchip, the whole arrangement was placed in a deep-UV/ozone exposure system (UVO cleaner model 342, Jelight Company Inc., Irvine, CA). A spatial filter was added to block radiations with large incident angles. If a coherent deep-UV source was to be used, then a spatial filter was not required. When UV radiations were transmitted through the microchip, ozone was formed by the 185 nm radiation in the air gap between the two glass slides. This ozone in combination with the 254 nm radiation converted hydrocarbons (the composition of OTS) into volatile molecules such as H_2O and CO_2. This process was responsible for the removal of OTS under deep-UV radiation. Irradiation time highly depends on air gap thickness, power density of the exposure system, and the distance between the lamp and the exposed target. As a reference, a typical exposure time for the UVO cleaner with a distance of 4 cm between the lamp and the target was around 4 h for a chip with 40–80 μm in thickness. These parameters were checked to ensure that the OTS was completely removed in the exposed regions to avoid any possible discrepancy in the experiments. After the UV exposure, the fabrication of the surface-guided microchannel was completed. When liquid was brought in contact with the reservoirs, capillary forces drove the fluid through the hydrophilic pathway to form a microchannel. Figure 3 shows a section of this microchannel.

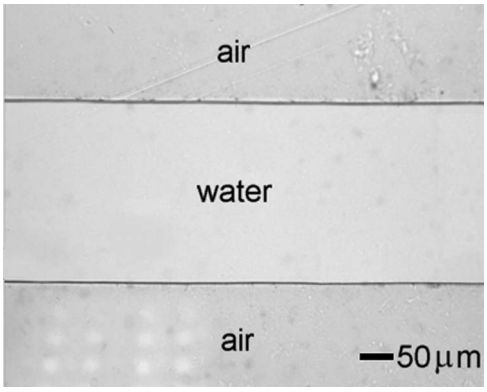

FIG. 3. Microchannel was fabricated using OTS and deep-UV exposure method. The sidewalls of this channel are the water-air interface. Channel's depth is 80 μm.

EXPERIMENTAL METHOD

The purpose of the experiments was to measure the electro-osmotic velocity profile in the presence of immiscible liquid-fluid interfaces. Two cases were tested. The first case was a water-air system and the second was a water-oil system. 0.5 μm fluorescence polystyrene particles (Molecular Probe Inc., Oregon) were used as trace particles for the velocity measurements. These particles were surfactant free and were coated with sulfate surface groups. The negative charges of the surface groups minimize the probability of the particles adhering to the channel wall. These particles were diluted in de-ionized (DI) water at a 0.5 % v/v ratio. De-ionized water was used as the working solution to enhance the thickness and the effects of the electrical double layer. The experimental setup consisted of a Leica DMLM fluorescent microscope, OPENLAB 3.1.5 image acquisition software, and an in-house built electrokinetic-flow control platform. Particle velocity was measured using particle streak images.[27–29] These images were taken by setting the exposure time of the image acquisition system to be between 50 and 100 ms. Only particles in the focusing plane were measured. Figure 4 shows a representative particle streak image used in the experiments. Particle velocities were obtained by measuring the length of the streak lines and dividing them by the exposure time. Twenty to fifty particle streak images were used to measure the particle velocity at different sections of the channel to construct the velocity profile in the microchannel. Since the goal of this study was to compare the shape of the velocity profiles between the experiments and proposed theories, the particle velocities, instead of real

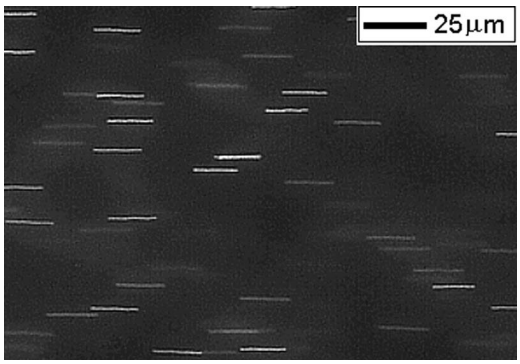

FIG. 4. An example of a particle streak image used to measure velocity profile. The image was captured with a 32× objective lens with an exposure time of 100 ms under an applied electric field of 50 V/cm. Microchip's depth is 80 μm.

fluid velocities, were used to construct the profile because they provided the same qualitative information. It should be noted that the real fluid velocity and the observed particle velocity are related by $u_{\text{fluid}}+\mu_{\text{ep}}E=u_{\text{ob}}$, where $\mu_{\text{ep}}E$ represents the electrophoresis of particles. For polystyrene particles dispersed in pure water, the electrophoretic mobility μ_{ep} is negative.

RESULTS AND DISCUSSIONS

Although many studies have been conducted on the electrical properties of liquid-fluid interfaces,[30–40] there was no study on how these properties affect electro-osmotic flow. Furthermore, Mbamala and von Grunberg[41] considered the existence of an electrostatic surface potential at the water-air interface to be controversial. They assumed the water-air interface to be neutral in their investigation on the effective interaction of charged colloidal particles at a water-air interface.

Three theoretical models are compared against two scenarios: electro-osmotic flow with water-air interface and water-oil interface (octane was used as the oil phase). In the analysis, the microchannel is 300 μm wide and 40–80 μm in depth. The zeta potential of glass/silica surfaces with deionized water solution is assumed to be −86 mV.[42] A zeta potential of −65 mV is used for the water-air interface,[36] and a zeta potential of −70 mV is assumed for the water-oil interface.[31] Other physical properties used in the analysis include the viscosity of water $\mu=1\times10^{-3}$ N s/m^2, the viscosity of air $\mu=1.8\times10^{-5}$ N s/m^2, and the viscosity of octane $\mu=5.66\times10^{-4}$ N s/m^2.

The first scenario considered here is electro-osmotic flow with a water-air interface. Figure 5 shows the experimental velocity measurements for an 80 μm deep channel under various applied electric field strengths and the prediction of the three theoretical models for an applied electric field strength of 100 V/cm. Figure 6 shows a particle streak image obtained in the experiments. It can be clearly seen from Figs. 5(a) and 6 that the experimental velocity profiles inside the microchannel remain pluglike, even near the proximity of the water-air interface. This observation is also consistent for a 40 μm deep channel. The particle velocity increases linearly with the applied electric field and this is expected because electro-osmotic flow velocity is known to be directly proportional to applied electric field.

From the comparisons between the experimental results

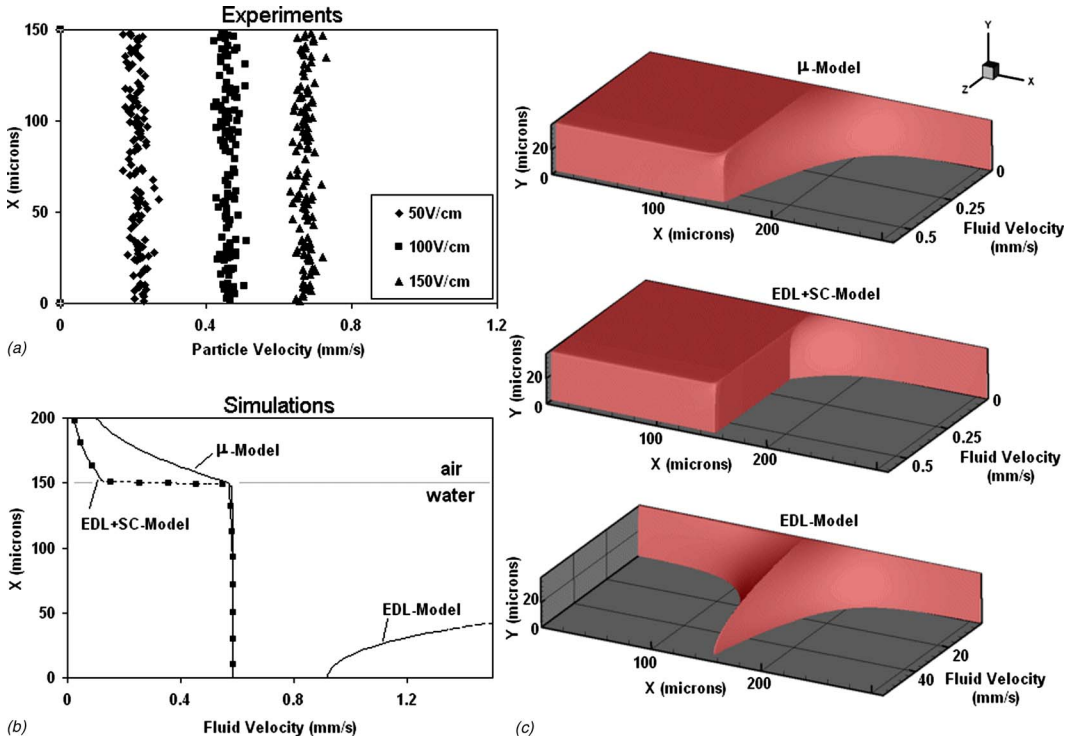

FIG. 5. (Color online) Experimental and numerical comparisons between the three theoretical models for the water-air system. (a) Experimental results for particle velocity in fluid 1 (water) for three different applied electric field strengths. (b) Numerical simulation results for the three theoretical models at $y=0$ μm under an applied electric field of 100 V/cm. (c) The three-dimensional views of the simulation results for the three theoretical models. Fluid 1 (water) ranges from $x=0$–150 μm and fluid 2 (air) ranges from $x>150$ μm.

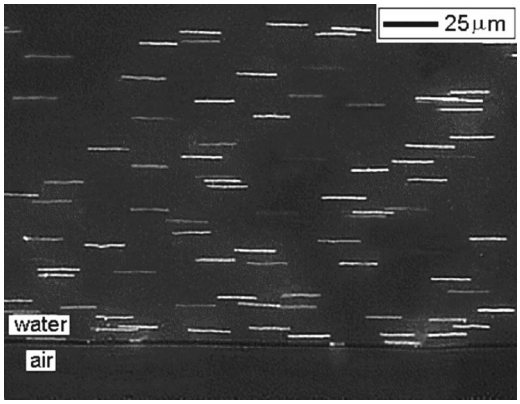

FIG. 6. A particle streak image for electro-osmotic flow near a water-air interface under an applied electric field of 50 V/cm. Microchannel's depth is 80 μm.

and the theoretical predictions, the EDL model stands out to be the most unmatched one. Considering the EDL model physically, the sharp increase in velocity is because the EDL forces accelerate the liquid at the interface, without direct counteracting forces. The counteracting forces come from the viscous drag from the top and bottom stationary glass surfaces. When the viscous forces are large enough to balance the EDL forces, the steady state liquid velocity at the water-air interface is already over tenfolds of the normal electro-osmotic velocity in the main flow. This result is highly skeptical and unreasonable.

The EDL is a direct consequence from the presence of the surface charges. In a normal glass microchannel (i.e., a microchannel with solid walls), the surface charges are immobile; therefore, the electrical interaction between the applied electric field and the surface charges can be neglected because it will not influence the liquid velocity at the solid surface. However, in the case studied here, the water-air interface is mobile. Forces acting on the surface charges at the liquid-fluid interface must be taken into consideration. Since the surface charges are located at the liquid-fluid interface,[33,35,37] the forces acting on these charges can be considered as surface forces. These surface forces should be included in the liquid-fluid interface boundary condition on the fluid flow, where the difference in shear stresses at the liquid-fluid interface is equal to the electrical surface stress due to the surface charges. This is the essence of the EDL +SC model.

It should be noted that both the μ model and EDL+SC model match the experimental results quite well qualitatively. Under an applied electric field of 100 V/cm, the predicted fluid velocities from the two models are higher than the experimentally measured particle velocity by roughly 0.1 mm/s. This difference may be due to the electrophoresis of the particles. By considering the surface charges in the EDL+SC model, the resulting velocity profile appears pluglike. Although the EDL forces try to accelerate the water molecules near the interface, the electrical surface forces, acting in the opposite direction, are dragging back the liquid at the interface. Because the forces acting on the surface charges are modeled as surface forces at the interface, mechanically it is similar to the shear forces applied at the interface. The shear forces acting at the liquid-fluid interface have similar effects to the shear forces acting at a solid-liquid interface, balancing the body forces in the EDL and producing a pluglike velocity profile. Furthermore, the simulation results also indicate that the velocity profile appears pluglike even for different zeta potentials (from 0 to -84 mV) for the water-air system. This phenomenon can be understood as follows. The surface charge density at the liquid-fluid interface ($\sigma_s = \vec{n} \cdot \varepsilon\varepsilon_0 \nabla_\psi|_{x=l}$) must balance the total net charge in the EDL by

$$\sigma_s = -\int_0^l \rho_e \, dx. \tag{9}$$

Therefore, the forces acting at the liquid-fluid interface and the forces acting in the EDL exactly balance each other regardless of the zeta potential. If the zeta potential is high, the local net charges and the surface charges will be correspondingly higher, and vice versa. Large EDL forces require large interfacial shear stresses, which are provided by the high surface charge density, to maintain a pluglike velocity profile. In contrast, at a low zeta potential, a pluglike profile can be maintained with low surface shear stresses, which are provided by the low surface charge density.

The μ model also shows a pluglike velocity profile inside the microchannel. This model can be easily understood because the interface can be considered as a stress free surface in the case of a water-air system. Since minimal stresses are applied on the liquid-fluid interface, the velocity at the interface remains the same as the bulk flow, preserving the pluglike profile. Although both the EDL+SC model and the μ model match the experimental results for a water-air system, these two models were tested with a second case with a promise to obtain further insights as to which model best describe the physical phenomena of electro-osmotic flow with a liquid-fluid interface.

Figure 7 shows the velocity profiles of electro-osmotic flow in a microchannel with a water-oil interface. From the experimental results, it can be clearly seen that the liquid velocity still appears to be pluglike. According to the simulations, this phenomenon can only be explained by the EDL+SC model. The EDL+SC model predicts a relatively pluglike profile for a system with a charged water-oil interface. In contrast, a paraboliclike profile at the midplane of the microchannel is predicted if the water-oil interface is electrically neutral. As shown in Figs. 7(b) and 7(c), there is a slight decrease in velocity near the water-oil interface. It is because the oil exerts an extra shear stress at the water-oil interface beside the shear stresses created by the surface charges. This decrease in velocity is not observed for the water-air system simulated by the EDL+SC model. This is simply because air exerts negligible stresses at the liquid-fluid interface (air's viscosity is much smaller). Not only do all the experimental results indicated the EDL+SC model as the more accurate model but the literature also provides ample evidence supporting this conclusion. Over past decades, researchers have been measuring the zeta potential of oil drops and air bubbles. The measurable values of zeta potential signify the existence of surface charges and the

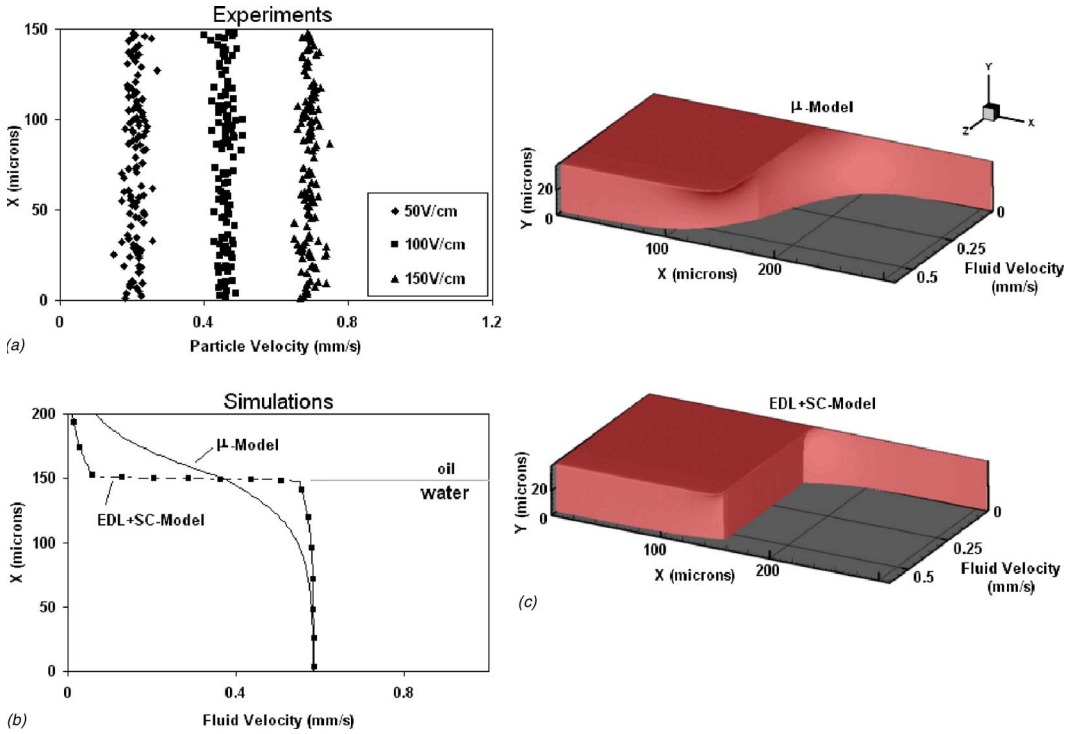

FIG. 7. (Color online) Experimental and numerical comparisons between the three theoretical models for the water-oil system. (a) Experimental results for particle velocity in fluid 1 (water) for three different applied electric field strengths. (b) Numerical simulation results for the two theoretical models at $y=0$ μm under an applied electric field of 100 V/cm. (c) The three-dimensional views of the simulation results for the two theoretical models. Fluid 1 (water) ranges from $x=0-150$ μm and fluid 2 (oil) ranges from $x>150$ μm.

EDL in those systems. There are a lot of evidence, both by experiments[30–32,36] and molecular dynamic simulations,[35,37] suggesting that the OH– and other negative ions in water are adsorbed onto water-air and water-oil interfaces. The accumulation of negative ions at the liquid-fluid interface is responsible for the arrival of surface charges at the interface, which, consequently, forms the electrical double layer. With the general acceptance of EDL formation at water-air and water-oil interfaces, the EDL+SC model is the only model out of the three that can explain the phenomena observed in our experiments, as well as concurring with previously developed theories and experimentations.

CONCLUSIONS

This paper presents a fundamental investigation on electro-osmotic flow involving immiscible liquid-fluid interfaces. In this work, we proposed a fabrication method that can create microchannels with immiscible liquid-fluid interfaces as the sidewalls. Using this channel, the particle velocity inside the microchannel was measured using the particle streak method. In order to gain understandings for the observed phenomena, three theoretical models were tested for two types of system: water-air and water-oil systems. We have experimentally demonstrated the model that incorporates the EDL theory along with the effects of surface charges best explains the physical phenomena. This finding is important because it provides the basis for future research in electrokinetic two-phase flow systems. The fabrication procedure that is proposed in this work is also significant because it provides a simple method for creating microchannels with immiscible liquid-fluid interfaces as the sidewalls.

ACKNOWLEDGMENTS

The authors are thankful for the financial support of the National Science and Engineering Research Consul of Canada through a research grant to one of the authors D.L and scholarships to two of the authors J.L. and I. B.-N.

[1] N. A. Patankar and H. H. Hu, Anal. Chem. **70**, 1870 (1998).
[2] D. Erickson and D. Li, Langmuir **19**, 5421 (2003).
[3] S. Arulanandam and D. Li, Colloids Surf., A **161**, 89 (2000).
[4] J. G. Santiago, Anal. Chem. **73**, 2353 (2001).
[5] L. Ren and D. Li, J. Colloid Interface Sci. **243**, 255 (2001).
[6] D. Sinton and D. Li, Colloids Surf., A **222**, 273 (2003).
[7] E. Biddiss, D. Erickson, and D. Li, Anal. Chem. **76**, 3208 (2004).
[8] V. Dolnik, S. R. Liu, and S. Jovanovich, Electrophoresis **21**, 41 (2000).
[9] C. S. Effenhauser, G. J. M. Bruin, and A. Paulus, Electrophoresis **18**, 2203 (1997).
[10] D. Sinton, C. Ren, and D. Li, J. Colloid Interface Sci. **260**, 431 (2003).
[11] I. Shestopalov, J. D. Tice, and R. F. Ismagilov, Astron. Tsirk. **4**, 316 (2004).
[12] K. D. Altria, J. Mod. Opt. **892**, 171 (2000).
[13] A. Marsh, B. Clark, M. Broderick, J. Power, S. Donegan, and K. Altria, Electrophoresis **25**, 3970 (2004).
[14] A. Brask, G. Goranovic, and H. Bruus, Proceedings of the NanoTech 2003, San Francisco, USA, 2003 (unpublished), Vol. 1, p. 190.
[15] M. Watanabe, H. Shirai, and H. Hirai, Sens. Actuators B **94**, 267 (2003).
[16] Y. Gao, T. N. Wong, C. Yang, and K. T. Ooi, J. Colloid Interface Sci. **284**, 306 (2005).
[17] B. Zhao, J. S. Moore, and D. J. Beebe, Langmuir **19**, 1873 (2003).
[18] B. Zhao, J. S. Moore, and D. J. Beebe, Anal. Chem. **74**, 4259 (2002).
[19] B. Zhao, J. S. Moore, and D. J. Beebe, Science **291**, 1023 (2001).
[20] S. Bouaidat, O. Hansen, H. Bruus, C. Berendsen, N. K. Bau-Madsen, P. Thomsen, A. Wolff, and J. Jonsmann, Astron. Tsirk. **8**, 827 (2005).
[21] Y. Gao, T. N. Wong, C. Yang, and K. T. Ooi, Colloids Surf., A **266**, 117

(2005).
[22]R. J. Hunter, *Zeta Potential in Colloids Science; Principles and Applications* (Academic, New York, 1981).
[23]K. S. Lee, G. B. Blanchet, F. Gao, and Y. L. Loo, Appl. Phys. Lett. **86**, 074102 (2005).
[24]Y. Masuda, S. Wakamatsu, and K. Koumoto, J. Eur. Ceram. Soc. **24**, 301 (2004).
[25]Y. N. Xia and G. M. Whitesides, Annu. Rev. Mater. Sci. **28**, 153 (1998).
[26]M. K. Ghantasala, J. P. Hayes, E. C. Harvey, and D. K. Sood, J. Micromech. Microeng. **11**, 133 (2001).
[27]J. A. Taylor and E. S. Yeung, Anal. Chem. **65**, 2928 (1993).
[28]T. E. McKnight, C. T. Culbertson, S. C. Jacobson, and J. M. Ramsey, Anal. Chem. **73**, 4045 (2001).
[29]A. D. Stroock, M. Weck, D. T. Chiu, W. T. S. Huck, P. J. A. Kenis, R. F. Ismagilov, and G. M. Whitesides, Phys. Rev. Lett. **84**, 3314 (2000).
[30]Y. Gu and D. Li, Colloids Surf., A **137**, 205 (1998).
[31]K. G. Marinova, R. G. Alargova, N. D. Denkov, O. D. Velev, D. N. Petsev, I. B. Ivanov, and R. P. Borwankar, Langmuir **12**, 2045 (1996).
[32]Y. Gu and D. Li, Colloids Surf., A **139**, 213 (1998).
[33]M. Vandentempel, J. R. Netherlands Chem. Soc. 72, 419 (1953).
[34]M. Paluch, Adv. Colloid Interface Sci. **84**, 27 (2000).
[35]B. C. Garrett, Science **303**, 1146 (2004).
[36]A. Graciaa, G. Morel, P. Saulner, J. Lachaise, and R. S. Schechter, J. Colloid Interface Sci. **172**, 131 (1995).
[37]M. Roeselova, J. Vieceli, L. X. Dang, B. C. Garrett, and D. J. Tobias, J. Am. Chem. Soc. **126**, 16308 (2004).
[38]A. Phianmongkhol and J. Varley, J. Colloid Interface Sci. **260**, 332 (2003).
[39]J. Stachurski and M. Michalek, J. Colloid Interface Sci. **184**, 433 (1996).
[40]A. Wiacek and E. Chibowski, Colloids Surf., A **159**, 253 (1999).
[41]E. C. Mbamala and H. H. von Grunberg, J. Phys.: Condens. Matter **14**, 4881 (2002).
[42]D. Erickson, D. Li, and C. Werner, J. Colloid Interface Sci. **232**, 186 (2000).